Parametric Imaging of Myocardial Blood Flow with ^{15}O-Water and PET Using the Basis Function Method

Hiroshi Watabe, PhD[1]; Hiroshi Jino, PhD[2]; Naoki Kawachi, PhD[3]; Noboru Teramoto, PhD[1]; Takuya Hayashi, MD, PhD[1]; Youichiro Ohta, BSc[1]; and Hidehiro Iida, DSc[1]

[1]Department of Investigative Radiology, National Cardiovascular Center Research Institute, Osaka, Japan; [2]Research Laboratories, Kyoto Pharmaceutical Industries, Ltd., Kyoto, Japan; and [3]SHI Accelerator Service Ltd., Tokyo, Japan

Regional myocardial blood flow (MBF) can be measured with ^{15}O-water and PET using the 1-tissue-compartment model with perfusable tissue fraction, which provides an MBF value that is free from the partial-volume effect. Studies with ^{15}O-water have several advantages, such as the ability to repeat a scan. However, because of the short scanning time and the small distribution volume of ^{15}O-water in the myocardium, the image quality of ^{15}O-water is limited, impeding the computation of MBF and perfusable tissue fraction at the voxel level. We implemented the basis function method for generating parametric images of MBF, perfusable tissue fraction, and arterial blood volume (V_a) with ^{15}O-water and PET. The basis function method linearizes the solution of the 1-tissue-compartment model, which results in a computationally much faster method than the conventional nonlinear least-squares fitting method in estimating the parameters. **Methods:** To validate the basis function method, we performed a series of PET studies on miniature pigs ($n = 7$). After acquisition of the transmission scan for attenuation correction and the ^{15}O-CO scan for obtaining the blood-pool image, repeated PET scans with ^{15}O-water were obtained with varying doses of adenosine or CGS-21680 (selective adenosine A_{2a} receptor agonist). MBF, perfusable tissue fraction, and V_a values of the myocardial region for each scan were computed using the basis function method and the nonlinear least-squares method, and the parameters estimated by the 2 methods were compared. **Results:** MBF images generated by the basis function method demonstrated an increase in blood flow after administration of adenosine or CGS-21680. The MBF values estimated by the basis function method and by the nonlinear least-squares method correlated strongly. **Conclusion:** The basis function method produces parametric images of MBF, perfusable tissue fraction, and V_a with ^{15}O-water and PET. These images will be useful in detecting regional myocardial perfusion abnormalities.

Key Words: myocardial blood flow; PET; ^{15}O-water; perfusable tissue fraction

J Nucl Med 2005; 46:1219–1224

A technique has been proposed to noninvasively measure regional myocardial blood flow (MBF) using ^{15}O-water and PET (*1–3*). The technique uses a single-tissue-compartment model, and its validity has been confirmed by several investigators, mostly by a comparison with microsphere experiments. One unique feature of this technique is that the model incorporates the concept of water-perfusable tissue fraction, which corrects the underestimation of MBF due to cardiac wall motion and the thinness of the myocardial wall relative to the intrinsic spatial resolution of the PET scanner. Therefore, the MBF value measured by this technique is independent of the PET camera (*4*). The use of ^{15}O-water with this technique offers several advantages (*5*), such as its short half-life (2 min), which enables easily repeated scans. Other advantages are that ^{15}O-water is metabolically inert and the synthesis of ^{15}O-labeled compounds is relatively easy. However, a disadvantage of this technique (*5*), compared with techniques using ^{13}N-ammonia (*6*), is that because of the short half-life of ^{15}O and the small distribution volume of ^{15}O-water in the myocardium, the tracer rapidly disappears. Consequently, the image quality is limited, making computation of MBF and perfusable tissue fraction at a voxel level by this technique extremely difficult because of the requirement of nonlinear least-squares fitting. Additionally, the myocardium cannot clearly be visualized because of the diffusibility of water.

Gunn et al. proposed a technique to produce the parametric image of binding potential for ^{11}C-raclopride (dopamine D_2 receptor ligand) using the basis function method (*7*). In this method, the nonlinear terms are first computed and the parameters of each voxel are linearly solved, making estimation of the parameters rapid.

We embraced the concept of the basis function method and implemented it to generate parametric images of MBF, perfusable tissue fraction, and arterial blood volume (V_a) with ^{15}O-water and PET. PET studies were performed on miniature pigs to evaluate the technique.

The theory of the method is as follows.

Received Sep. 7, 2004; revision accepted Mar. 17, 2005.

For correspondence or reprints contact: Hiroshi Watabe, PhD, Department of Investigative Radiology, National Cardiovascular Center Research Institute, 5-7-1 Fujishirodai, Suita, Osaka 565-8565.

E-mail: watabe@ri.ncvc.go.jp

The tissue activity curve of the myocardial region observed by PET (Dm(t) [cps/mL]) after the administration of ^{15}O-water can be expressed using $MBF_p(f)$ (mL/min/g of perfusable tissue), perfusable tissue fraction (a) (g/mL), and V_a fraction (mL/mL) as follows (*2*):

$$D_m(t) = \alpha f C_a(t) \otimes \exp\left(- \left(\frac{f}{p} + \lambda\right)t\right) + V_a C_a(t), \quad \text{Eq. 1}$$

where $C_a(t)$ (cps/mL) is the arterial input function, p is the tissue/blood partition coefficient (assuming a constant of 0.91 mL/g (*1*)), and λ is the physical decay constant of ^{15}O (0.00567 s^{-1}). $\otimes$ denotes the convolution operation. $D_m(t)$ and $C_a(t)$ in Equation 1 are not corrected for the physical decay of ^{15}O. The 3 parameters f, α, and V_a can be estimated by fitting to Equation 1 using the nonlinear least-squares method.

In the basis function method, the nonlinear term in Equation 1 is linearized and Equation 1 is rewritten as follows:

$$D_m(t) = \theta_1 C_a(t) + \theta_2 C_a(t) \otimes e^{-\theta_3 t}, \quad \text{Eq. 2}$$

where $\theta_1 = V_a$, $\theta_2 = \alpha f$, and $\theta_3 = f/p + \lambda$. The nonlinear term in Equation 2 including θ_3 is precalculated as the discrete basis function $B_i(t)$ for the available range of θ_3:

$$B_i(t) = C_a(t) \otimes e^{-\theta_3 t}. \quad \text{Eq. 3}$$

Using the basis function $B_i(t)$, Equation 2 becomes:

$$D_m(t) = \theta_1 C_a(t) + \theta_2 B_i(t). \quad \text{Eq. 4}$$

Solving Equation 4 is a linear problem against the parameters θ_1 and θ_2. For each basis function, θ_1 and θ_2 in Equation 4 are estimated by means of the linear least-squares technique. θ_3 is determined by searching the minimum sum of squared residuals between the estimated and observed data among all basis functions. From the determined θ_1, θ_2, and θ_3 values, MBF_p, perfusable tissue fraction, and V_a can be calculated as $f = (\theta_3 - 1)\cdot p$, $\alpha = \theta_2/f$, and $V_a = \theta_1$. These computations are done for each voxel, and parametric images of MBF_p, MBF_t ($MBF_p \cdot \alpha$), perfusable tissue fraction (α), and V_a are generated.

In this study, the range of θ_3 was set to 0.00567 (decay constant of ^{15}O) $< \theta_3 \leq 0.1$, and 300 discrete basis functions were generated.

Because of heart motion and the limited spatial resolution of PET, the arterial input function, Ca(t) in Equations 1 and 3, cannot be derived directly from the PET image. To obtain Ca(t), we used the following equations (*2,3*):

$$D_m(t) = \left(\frac{\alpha}{\beta} - \frac{1-\beta}{\beta^2}\cdot V_a\right)\cdot f \cdot D_l(t) \otimes e^{-((1/p)+(1-\beta)/\beta)f+\lambda)t} + \frac{V_a}{\beta} D_l(t) \quad \text{Eq. 5}$$

$$C_a(t) = \frac{1}{\beta} D_l(t) - \frac{1-\beta}{\beta^2} f \cdot D_l(t) \otimes e^{-((1/p)+(1-\beta)/\beta)f+\lambda)t}, \quad \text{Eq. 6}$$

where $D_l(t)$ is the tissue activity curve for the left ventricle and β is the recovery coefficient of the left ventricular region of interest (ROI) ($0.0 < \beta \leq 1.0$). To obtain $D_m(t)$ and $D_l(t)$, we drew ROIs on the left ventricle and the myocardium. By fitting $D_m(t)$ to Equation 5, we estimated f, α, and V_a. Using the estimated parameters, Ca(t) was computed using Equation 6.

MATERIALS AND METHODS

Subjects

To validate the present technique, we performed PET studies on 7 miniature pigs (6 mo old, weighing 16.5–21.0 kg). The pigs were anesthetized by introduction of pentobarbital followed by continuous inhalation of propofol (4 mg/kg/h) and were placed supine on the bed of the scanner.

PET Scanning

The scanner used was an ECAT EXACT HR (CTI/Siemens) (*8*), which has an imaging field of view 55 cm in diameter and 15 cm in axial length. The spatial resolution of the scanner is 5.8 mm in full width at half maximum at the center of the field of view. After obtaining a 10-min transmission scan for attenuation correction, we obtained a blood-pool image with a 4-min PET scan after a 30-s inhalation of 2.7 GBq ^{15}O-CO by the pigs. Arterial blood samples were taken every minute during the ^{15}O-CO scanning, and the radioactivity concentration in the whole blood was measured using a NaI well counter, which was calibrated against the PET scanner. Subsequently, 14 or 15 PET scans with ^{15}O-water were obtained with administration of various doses of adenosine or the selective adenosine A_{2a} receptor agonist CGS-201680 (*9*) (6 scans with adenosine [25, 50, 100, 200, 400, and 800 mg/kg/min] and 6 scans with CGS-21680 [0.5, 1, 2, 5, 10, and 20 μg/kg], with the addition of 2 or 3 scans under resting conditions). The total number of PET scans with ^{15}O-water was 100 for the 7 pigs. The interval between scans was more than 15 min to allow for physical decay of ^{15}O radioactivity to the background level. ^{15}O-water was injected into the right femoral vein for 30 s at an infusion rate of 10 mL/min (injected radioactivity was about 700 MBq). Immediately after injection of water, PET data were acquired for 6 min, with 26 dynamic frames: 12 × 5 s, 8 × 15 s, and 6 × 30 s. All acquisitions were in 2-dimensional mode (septa extended).

Additional scanning was performed in list mode on a miniature pig for 6 min. The scan was obtained under resting condition. This dataset was used to evaluate the voxelwise noise property of the functional images produced by the technique.

Image Processing

A filtered backprojection algorithm with a 6-mm gaussian filter was used for image reconstruction. The reconstructed images had a matrix size of 128 × 128 × 47 and a voxel size of 1.84 × 1.84 × 3.38 mm, and all image datasets were resliced into short-axis images with 20 slices across the left ventricle.

For the list-mode dataset, each event of the list-mode data was normalized, correcting for both detector efficiency and geometry, as well as crystal interference (*10*). Then, the list-mode data were sorted into 30 subsinogram datasets, and 10 replicated sinogram datasets were generated from the subsinogram datasets using the nonparametric bootstrap technique (*11*). Each set of sinogram data was reconstructed in the manner previously described. The obtained images thus represented 10 statistically independent replicates of the scan.

Data Analysis

All data analysis was performed on a personal computer (Linux operating system [version 2.4.18] installed on a 2.2-GHz Pentium 4 processor [Intel Corp.] with 1 GB of memory). The interactive modeling and data analysis system called BLD (*12*) (porting to Linux) was used to estimate parameters by the nonlinear least-squares method. Programming for the basis function method was written in C language (version 3.2; GNU Compiler Collection).

Templates of ROIs for the left ventricle and the myocardium were drawn on the blood-pool image with ^{15}O-CO and washout phase of water (average ROI sizes for the 7 pigs were 0.922 ± 0.313 cm^3 and 9.80 ± 2.56 cm^3 for left ventricle and myocardium, respectively). The templates of the ROIs were superimposed on the dataset for each scan, and tissue activity curves for the left ventricle and the myocardium were generated for each scan. The 4 parameters MBF_t, MBF_p, α, and V_a for the myocardium were estimated by using the 2 tissue activity curves and fitting to Equation 5 by means of the nonlinear least-squares method. Further, the 2 tissue activity curves were used to estimate the arterial input function $C_a(t)$ using Equation 6. To avoid computing the unwanted region (such as liver), we generated a mask image from the washout image by thresholding 50% of the voxel value. The estimated $C_a(t)$ was used for the basis function method, and the parametric images of MBF_t, MBF_p, perfusable tissue fraction, and V_a were generated. Average values of the parameters inside the ROI template for the myocardium were computed for each parametric image, and these values were compared with the estimated parameters using the nonlinear least-squares method.

For the list-mode dataset, from the 10 statistically independent replicates of the images, 10 functional images of MBF_t, MBF_p, perfusable tissue fraction, and V_a by the basis function method were computed. The voxelwise mean image and coefficient-of-variance image were then produced.

To evaluate the computational benefits of the basis function method against the nonlinear least-squares method, we analyzed 1 dynamic image of a pig (under resting condition) in depth. Five hundred voxels were randomly chosen in the heart region, and 500 tissue activity curves were taken from each voxel. Using the input function and the tissue activity curves, we estimated MBF_t, MBF_p, perfusable tissue fraction, and V_a using the nonlinear least-squares method. We also computed the parametric maps for the corresponding voxels using the basis function method. These calculations were repeated 10 times, and the computation times for the 2 methods were compared.

RESULTS

Figure 1 shows examples of parametric images of MBF_t, MBF_p, perfusable tissue fraction, and V_a under resting condition and under a 1 or 5 μg/kg/min dose of CGS-21680. It took about 90 s to produce parametric images of MBF_t, MBF_p, perfusable tissue fraction, and V_a (51,512 voxels for each image). As shown in this figure, MBF_t and MBF_p images clearly depicted the myocardial region and MBF_t, and MBF_p values increased as the dose of CGS-21680 increased. On the other hand, perfusable tissue fraction and V_a values stayed constant between scans. Figure 2 and Table 1 compare the parameters as estimated by the basis function method and by the nonlinear least-squares method. As shown in this figure, all parameters estimated by the 2 methods correlated strongly.

Figure 3 shows the mean images and coefficient-of-variance images of MBF_t, MBF_p, perfusable tissue fraction, and V_a computed using the basis function method and the nonparametric bootstrap technique. The averaged coefficient-of-variance percentages inside the ROI (3,210 voxels, 10.1 cm^3) placed on the myocardium were 14.2%, 16.2%, 5.27%, and 29.9% for MBF_t, MBF_p, perfusable tissue fraction, and V_a, respectively.

For the nonlinear least-squares method, it took 66.1 ± 4.6 s to compute MBF_t, MBF_p, perfusable tissue fraction, and V_a for the 500 voxels. In 35% of the 500 voxels, the nonlinear least-squares method aborted the estimation before the convergence. The basis function method completed computation of the parametric map for the 500 voxels in 3.4 ± 0.8 s (20 times faster than the nonlinear least-squares method).

DISCUSSION

In this paper, we have presented an approach to producing quantitative MBF and perfusable tissue fraction images using ^{15}O-water and PET. The basis function method has 2 main advantages over the nonlinear least-squares method. One is the ability to produce a voxel-by-voxel quantitative parametric map, and the other is faster computing speed. We are currently studying the use of ^{15}O-water and PET to

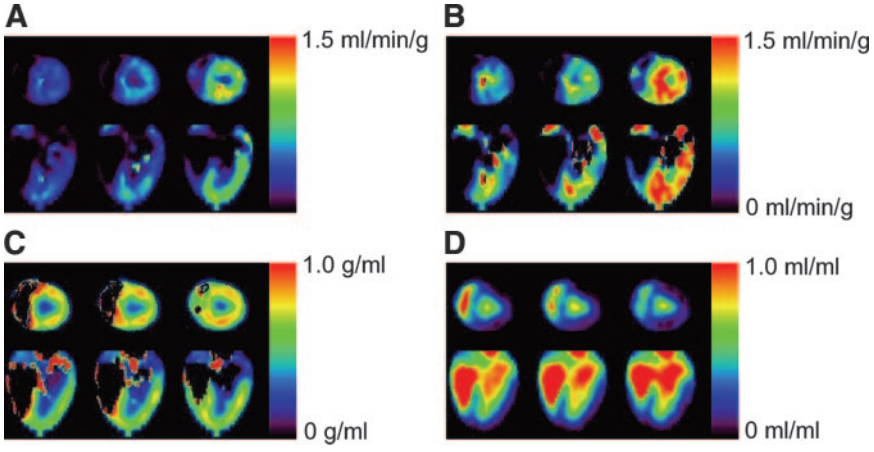

FIGURE 1. Examples of parametric images of MBF_t (A), MBF_p (B), perfusable tissue fraction (C), and V_a (D) under resting conditions (left) and under a 1 μg/kg/min (center) or 5 μg/kg/min (right) dose of CGS-21680.

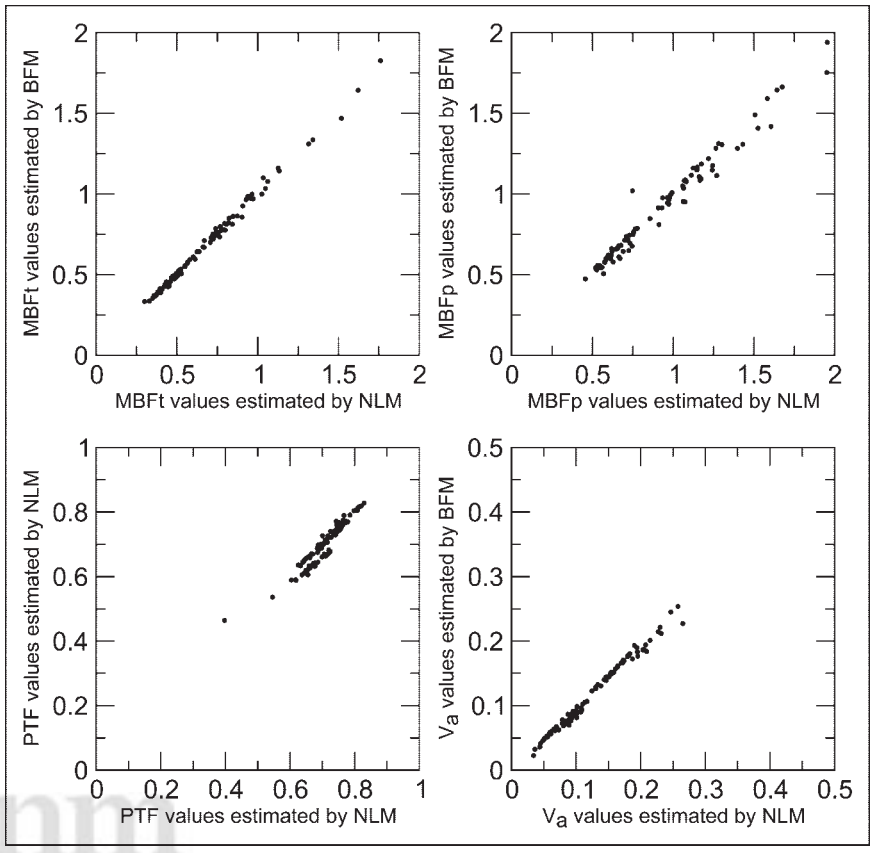

FIGURE 2. Comparison of MBF_t (top left), MBF_p (top right), perfusable tissue fraction (bottom left), and V_a (bottom right) values estimated using nonlinear least-squares method (NLM) with those estimated using basis function method (BFM).

evaluate skeletal myoblast transplantation for repair of myocardial necrosis in pigs. In these studies, 1 pig is scanned repeatedly under different conditions. For these studies, voxel-by-voxel analysis is preferred to ROI-based analysis because the operator can independently define ROIs to improve reproducibility, and faster computations are important for analyzing plenty of datasets.

Kinetic parameters estimated by the nonlinear least-squares method agreed well with those estimated by the basis function method, as shown in Figure 2. Although superior to the nonlinear least-squares method in terms of computing speed and ability to generate parametric maps, the basis function method shares the same source of errors as the nonlinear least-squares method because they use the same model and assumption. For instance, assumption of a constant value of 0.91 mL/g for the partition coefficient of water might be a problem, especially for diseased tissue. Motion of a patient during a study (*13*), flow heterogeneity (*14*), and spillover from the right ventricle (*15*) are sources of error for parameters estimated by both the nonlinear least-squares method and the basis function method. Using the nonlinear least-squares method, Iida et al. (*3*) reported that as the noise level increases, the statistical fluctuation and the systematic bias in the estimated parameters increase. This phenomenon could occur in the parameters estimated by the basis function method. To suppress the statistical fluctuation and the systematic bias, one must increase count statistics on each voxel. Although our study, shown in Figure 3, indicates that the statistical fluctuations on the functional images by the basis function method are within an acceptable range, further consideration is required to apply the basis function method to a human study because image quality is worse in studies on humans than in studies on miniature pig. Three-dimensional acquisition is a possible approach to increasing count statistics (*16*), although quantification of MBF in 3-dimensional acquisitions is still a question (*17*). The analytic model can be modified to improve the accuracy of the basis function method. For instance, Hermansen et al. (*15*) proposed a model that included spillover from both the left and the right ventric-

TABLE 1
Parameters Estimated with PET Using the 2 Methods for 7 Miniature Pigs

Parameter	Nonlinear least-squares method	Basis function method
MBF_t (mL/min/g)	0.801 ± 0.524	0.810 ± 0.528
MBF_p (mL/min/g)	1.14 ± 0.77	1.12 ± 0.73
Perfusable tissue fraction (g/mL)	0.708 ± 0.06	0.699 ± 0.068
V_a (mL/mL)	0.125 ± 0.057	0.118 ± 0.055

Total number of PET scans was 100.

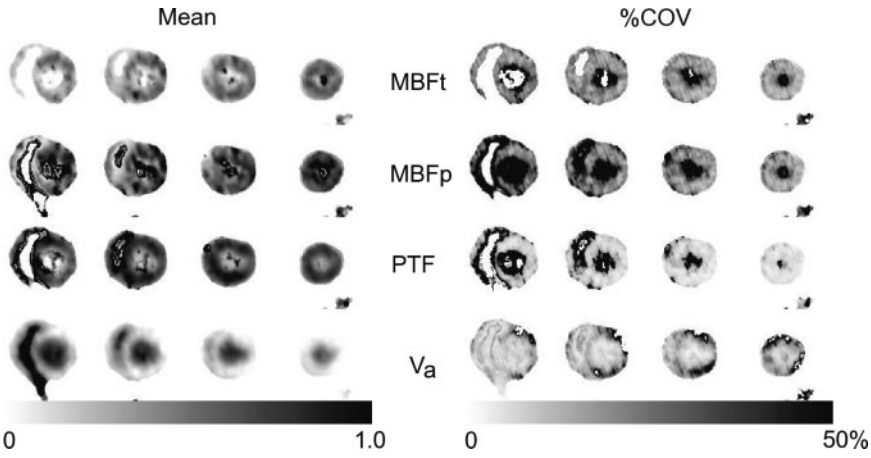

FIGURE 3. Four representative slices of functional images (MBF_t, MBF_p, perfusable tissue fraction [PTF], and V_a) obtained by basis function method (BFM) and nonparametric bootstrap technique. Mean images (left) and coefficient-of-variance images (%COV, right) were generated from 10 statistically independent replicates.

ular cavities with 4 parameters. Their approach is easily adapted to the basis function method, although the increased number of estimated parameters (from 3 to 4) might increase the error of the parameters.

Because the basis function method produces voxel-based functional images, quantification errors caused by subject motion might be more severe with this method than with the ROI-based technique. Although several techniques have corrected for subject motion during brain PET (*18–20*), motion correction during heart PET is still challenging because of the required nonrigid or nonlinear transformation of images.

Voxel-based perfusable tissue index can be calculated using the perfusable tissue fraction image, the basis function method, and the anatomic tissue fraction (*21*). The perfusable tissue index is theoretically unaffected by partial-volume effects and wall motion and could be a marker of viable myocardium (*22*). However, using computer simulations, Herrero et al. (*14*) demonstrated that flow heterogeneity caused the perfusable tissue index to be underestimated. Compared with the ROI-based perfusable tissue index, the voxel-based perfusable tissue index obtained by the basis function method could minimize flow heterogeneity, suppressing the bias on the perfusable tissue index. On the other hand, misalignment between the transmission image, CO image, and water image could produce a significant error in the voxel-based perfusable tissue index. Moreover, Iida et al. pointed out that spillover artifacts on the anatomic tissue fraction produced the error in the perfusable tissue index (*13*). A detailed comparison between the perfusable tissue index image and the histologic image will be required to investigate the feasibility of the voxel-based perfusable tissue index.

The present method requires the operator to draw the ROI on the left ventricular and myocardial regions to obtain the arterial input function, possibly resulting in an additional source of error. Factor analysis (*23*) is an attractive approach to decreasing the effect of operator variability. Alternatively, the arterial input function can be obtained from the aortic region (*24*).

The inverse of the Fisher information matrix (*25*) can be used to evaluate the noise in the functional images. However, this approach relies on the definition of the compartment model, and the high random and scatter counts in the heart PET study might distort the statistical distribution in the PET image. Thus, we used list-mode acquisition and the nonparametric bootstrap technique to estimate noise.

Compared with a study on miniature pigs, a study on humans would encounter worse problems if the basis function method were applied, because of the deterioration of the raw data (i.e., fewer count statistics and increased photon scatter, random coincidences, and attenuation). New generations of PET detectors (new crystals and faster electronics) are expected to help overcome these problems.

CONCLUSION

The basis function method was implemented to generate parametric images of MBF, perfusable tissue fraction, and blood volume with ^{15}O-water and PET. The method could compute the parametric images much more quickly than could the conventional nonlinear fitting approach. The MBF image and the perfusable tissue fraction image with ^{15}O-water may give additional information on the detection of regional myocardial perfusion abnormalities.

ACKNOWLEDGMENTS

This study was supported by the Program for Promotion of Fundamental Studies in Health Science of the Organization for Pharmaceutical Safety and Research (of Japan).

REFERENCES

1. Iida H, Kanno I, Takahashi A, et al. Measurement of absolute myocardial blood flow with $H_2{}^{15}O$ and dynamic positron-emission tomography strategy for quantification in relation to the partial-volume effect. *Circulation.* 1988;78:104–115.
2. Iida H, Rhodes CG, Silva R, et al. Myocardial tissue fraction: correction for partial volume effects and measure of tissue viability. *J Nucl Med.* 1991;32:2169–2175.
3. Iida H, Rhodes CG, Silva R, et al. Use of the left ventricular time-activity curve as a non-invasive input function in dynamic oxygen-15-water positron emission tomography. *J Nucl Med.* 1992;33:1669–1677.
4. Iida H, Yokoyama I, Agostini D, et al. Quantitative assessment of regional

myocardial blood flow using oxygen-15-labelled water and positron emission tomography: a multicentre evaluation in Japan. *Eur J Nucl Med.* 2000;27:192–201.
5. Huang SC, Schwaiger M, Carson RE, et al. Quantitative measurement of myocardial blood flow with oxygen-15 water and positron computed tomography: an assessment of potential and problems. *J Nucl Med.* 1985;26:616–625.
6. Choi Y, Huang SC, Hawkins RA, et al. Quantification of myocardial blood flow using ^{13}N-ammonia and PET: comparison of tracer models. *J Nucl Med.* 1999; 40:1045–1055.
7. Gunn RN, Lammertsma AA, Hume SP, et al. Parametric imaging of ligand-receptor binding in PET using a simplified reference region model. *Neuroimage.* 1997;6:279–287.
8. Wienhard K, Dahlbom M, Eriksson L, et al. The ECAT EXACT HR: performance of a new high resolution positron scanner. *J Comput Assist Tomogr.* 1994;18:110–118.
9. Hutchison AJ, Webb RL, Oei HH, et al. CGS 21680C, an A2 selective adenosine receptor agonist with preferential hypotensive activity. *J Pharmacol Exp Ther.* 1989;251:47–55.
10. Casey ME, Gadagkar H, Newport D. A component based method for normalization in volume PET. In: Grangeat P, Amans J-L, eds. *Third International Conference on Three-Dimensional Image Reconstruction in Radiology and Nuclear Medicine (Computational Imaging and Vision).* New York, NY: Kluwer Academic Publishers; 1996:67–71.
11. Buvat I. Non-parametric bootstrap approach for analysing the statistical properties of SPECT and PET images. *Phys Med Biol.* 2002;47:1761–1775.
12. Carson RE. Parameter estimation in positron emission tomography. In: Phelps ME, Mazziotta JC, Schelbert HR, eds. *Positron Emission Tomography and Autoradiography: Principles and Applications for the Brain and Heart.* New York, NY: Raven Press; 1986:347–390.
13. Iida H, Tamura Y, Kitamura K, et al. Histochemical correlates of ^{15}O-water-perfusable tissue fraction in experimental canine studies of old myocardial infarction. *J Nucl Med.* 2000;41:1737–1745.
14. Herrero P, Staudenherz A, Walsh JF, et al. Heterogeneity of myocardial perfusion provides the physiological basis of perfusable tissue index. *J Nucl Med.* 1995; 36:320–327.
15. Hermansen F, Rosen SD, Fath-Ordoubadi F, et al. Measurement of myocardial blood flow with oxygen-15 labelled water: comparison of different administration protocols. *Eur J Nucl Med.* 1998;25:751–759.
16. Schafers KP, Spinks TJ, Camici PG, et al. Absolute quantification of myocardial blood flow with $H_2{}^{15}O$ and 3-dimensional PET: an experimental validation. *J Nucl Med.* 2002;43:1031–1040.
17. Lammertsma AA. Myocardial perfusion in 3 dimensions. *J Nucl Med.* 2002;43: 1041–1043.
18. Fulton RR, Meikle SR, Eberl S, et al. Correction for head movements in positron emission tomography using an optical motion-tracking system. *IEEE Trans Nucl Sci.* 2002;49:116–123.
19. Bloomfield PM, Spinks TJ, Reed J, et al. The design and implementation of a motion correction scheme for neurological PET. *Phys Med Biol.* 2003;48:959–978.
20. Woo SK, Watabe H, Choi Y, et al. Sinogram-based motion correction of PET images using optical motion tracking system and list-mode data acquisition. *IEEE Trans Nucl Sci.* 2004;51:782–788.
21. Rhodes CG, Wollmer P, Fazio F, et al. Quantitative measurement of regional extravascular lung density using positron emission and transmission tomography. *J Comput Assist Tomogr.* 1981;5:783–791.
22. Knaapen P, Boellaard R, Gotte MJ, et al. The perfusable tissue index: a marker of myocardial viability. *J Nucl Cardiol.* 2003;10:684–691.
23. Hermansen F, Ashburner J, Spinks TJ, et al. Generation of myocardial factor images directly from the dynamic oxygen-15-water scan without use of an oxygen-15-carbon monoxide blood-pool scan. *J Nucl Med.* 1998;39:1696–1702.
24. Watabe H, Channing MA, Riddell C, et al. Noninvasive estimation of the aorta input function for measurement of tumor blood flow with [^{15}O]water. *IEEE Trans Med Imaging.* 2001;20:164–174.
25. Aston JA, Gunn RN, Worsley KJ, et al. A statistical method for the analysis of positron emission tomography neuroreceptor ligand data. *Neuroimage.* 2000;12: 245–256.

The Journal of NUCLEAR MEDICINE

Parametric Imaging of Myocardial Blood Flow with ^{15}O-Water and PET Using the Basis Function Method

Hiroshi Watabe, Hiroshi Jino, Naoki Kawachi, Noboru Teramoto, Takuya Hayashi, Youichiro Ohta and Hidehiro Iida

J Nucl Med. 2005;46:1219-1224.

The Journal of Nuclear Medicine is published monthly.
SNMMI | Society of Nuclear Medicine and Molecular Imaging
1850 Samuel Morse Drive, Reston, VA 20190.
(Print ISSN: 0161-5505, Online ISSN: 2159-662X)

SNMMI SOCIETY OF NUCLEAR MEDICINE AND MOLECULAR IMAGING